SARS-CoV2 infection triggers inflammatory conditions and astrogliosis-related gene expression in long-term human cortical organoids

Mathilde Colinet, Ioana Chiver, Dr, Antonela Bonafina, Dr, Gérald Masset, Daniel Almansa, Emmanuel Di Valentin, Dr, Jean-Claude Twizere, Dr, Laurent Nguyen, Dr, Ira Espuny-Camacho, Dr

SARS-CoV2 infection triggers inflammatory conditions and astrogliosis-related gene expression in long-term human cortical organoids

Mathilde Colinet[1], Dr. Ioana Chiver[1], Dr. Antonela Bonafina[1], Gérald Masset[1], Daniel Almansa[1], Dr. Emmanuel Di Valentin[2], Dr. Jean-Claude Twizere[3], Dr. Laurent Nguyen[1,4,5]* and Dr. Ira Espuny-Camacho[1,5]*

[1]Laboratory of Molecular Regulation of Neurogenesis, GIGA Institute, University of Liège, C.H.U. Sart Tilman, Liège 4000, Belgium.

[2]GIGA Viral Vector Platform, GIGA Institute, University of Liège, C.H.U. Sart Tilman, Liège 4000, Belgium.

[3]Laboratory of Viral Interactomes, Unit of Molecular Biology of Diseases, GIGA Institute, University of Liège, C.H.U. Sart Tilman, Liège 4000, Belgium.

[4]WELBIO department, WEL Research Institute, Avenue Pasteur, 6, Wavre 1300, Belgium.

[5]Co-last authors

*Corresponding Laurent Nguyen; Ira Espuny-Camacho, GIGA Institute, University of Liège, 400, Belgium (lnguyen@uliege.be, im.espunycamacho@uliege.be).

ABSTRACT

SARS-CoV2, severe acute respiratory syndrome coronavirus 2, is frequently associated with neurological manifestations. Despite the presence of mild to severe CNS-related symptoms in a cohort of patients, there is no consensus whether the virus can infect directly brain tissue or if the symptoms in patients are a consequence of peripheral infectivity of the virus. Here, we use long-term human stem cell-derived cortical organoids to assess SARS-CoV2 infectivity of brain cells and unravel the cell-type tropism and its downstream pathological effects. Our results show consistent and reproducible low levels of SARS-CoV2 infection of astrocytes, deep projection neurons, upper callosal neurons and inhibitory neurons in 6 months human cortical organoids. Interestingly, astrocytes showed the highest infection rate among all infected cell populations that led to changes in their morphology and upregulation of SERPINA3, CD44 and S100A10 astrogliosis markers. Further, transcriptomic analysis revealed overall changes in expression of genes related to cell metabolism, astrogliosis and, inflammation and further, upregulation of cell survival pathways. Thus, local and minor infectivity of SARS-CoV2 in the brain may induce widespread adverse effects and lead to resilience of dysregulated neurons and astrocytes within an inflammatory environment.

Keywords: Astrogliosis; human cortical organoids; inflammatory and cell survival mechanisms; SARS-CoV2 brain infectivity.

Graphical abstract

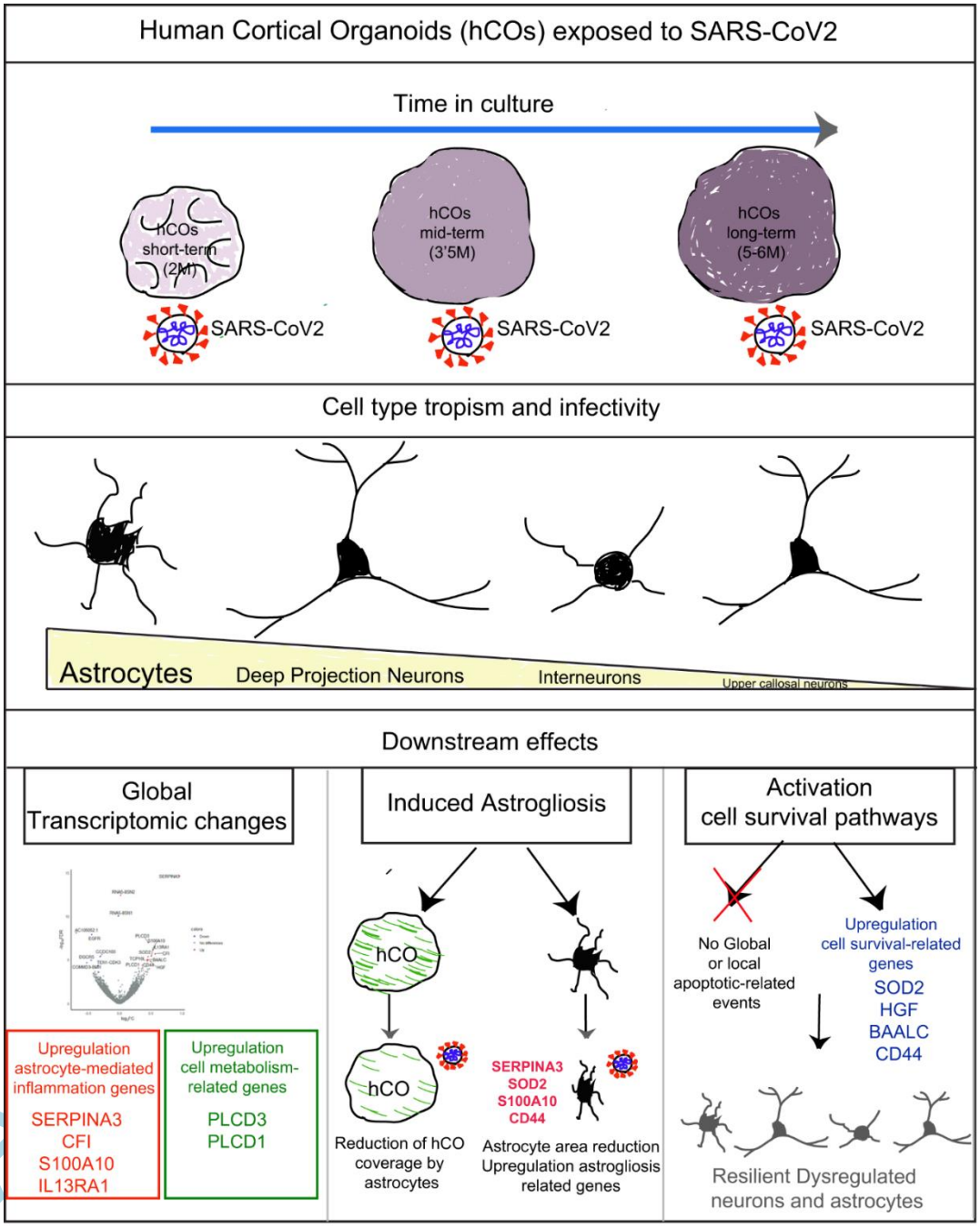

SIGNIFICANCE STATEMENT

Neurological-related symptoms are present in a subset of COVID19 patients, however it is not yet clear whether SARS-CoV2 can directly infect the human brain and which are the direct downstream effects. In this study we show that SARS-CoV2 can infect at low levels astrocytes and neurons from long-term cultured human cortical organoids. SARS-CoV2 infection leads to astrogliosis and triggers global gene expression changes related to inflammation, cell metabolism, and cell survival. These findings suggest that SARS-CoV2 infection may lead to the appearance of resilient dysregulated astrocytes and neurons in the brain.

INTRODUCTION

SARS-CoV2, severe acute respiratory syndrome coronavirus 2, that causes coronavirus disease 2019 (COVID-19), is associated with a plethora of symptoms in patients ranging from mild fever to pneumonia and, in a small proportion of cases, systemic defects that can lead to the death of the individual[1–4]. Recent findings have associated SARS-CoV2-infectivity related effects with alterations in multiple organs including lung, heart, kidney and brain. While SARS-CoV2 mainly targets the respiratory system, neurological manifestations have also been detected in patients. These neurological adverse effects include anosmia, strokes, seizures and impaired consciousness, among others[5–8]. Despite the observation of brain related symptoms in a fraction of the patients, the analysis of postmortem brains or cerebral spinal fluid (CSF) samples from surviving patients has led to contradictory results with most reports failing to detect the presence of SARS-CoV2 particles[9–13]. These observations suggest either low levels of infection in brain tissue or on the contrary an absence of infectivity in the brain, where neurological-related effects would rely on SARS-CoV2 peripheral organ infection.

SARS-CoV2 viral entry has been proposed to be mediated by the binding of the virus spike S protein to the receptor angiotensin converting enzyme 2 (ACE2) in the target cell. This event is followed by the activation of the spike S protein upon cleavage enacted by the host proprotein convertase furin and by membrane-associated serine proteinases (MASPs)[14,15], which leads to the fusion of the virus membrane with the host cell membrane[2,16]. Whereas high levels of ACE2 expression have been detected in major target tissues of SARS-CoV2 infection such as lung, kidney and heart, ACE2 levels are reported to be low or undetectable in the brain[17]. However, the expression of ACE2 co-receptors that potentiate SARS-CoV2 infectivity has been reported in several tissues, including the brain. These co-receptors include neuropilin 1 (NRP1) cell

surface receptor[16,18–20], dipeptidyl peptidase 4 (DPP4)[21], tyrosine-protein kinase receptor UFO (AXL)[22], extracellular matrix metalloproteinase inducer (CD147/BSG)[7,23,24] and endoplasmic reticulum (ER) stress-inducible chaperone BiP (GRP78/HSPA5)[25,26]. These reports support the possibility that alternative receptors and co-receptors are mediating SARS-CoV2 entry in brain cells.

Concerning the downstream effects of SARS-CoV2 infectivity, recent reports performing multi-organ screenings by magnetic resonance imaging (MRI) have detected multiple anomalies in lungs and brain in a cohort of COVID-19 patients 6 months post-infection[27]. In addition, postmortem analysis of patient brain tissue has revealed broad cellular perturbations of most cell types by single-cell transcriptomic[28] and proteomic[9] analysis. These studies suggested the preferential infectivity of astrocyte glial-cells and their consequent dysregulated homeostatic pathways linked to higher levels of inflammation detected in the brain. Whereas most studies have been focused on adult brain, a recent report has shown hemorrhagic phenotypes in the cortex of human fetuses exposed to SARS-CoV2[29], through a mechanism related to reduction in blood vessel integrity[29–31]. Several studies have used human pluripotent stem cell-derived brain organoids to analyze the infectivity of SARS-CoV2 in the brain and its pathological downstream effects. Infectivity of brain cell types has been reported to be low compared to the levels of infection detected for instance in models including choroid plexus epithelial and ependymal cells[32,33] and perivascular pericyte-like cells[34]. A few studies have corroborated *in vitro* the infectivity of astrocytes by SARS-CoV2 in agreement with the reports from postmortem brain sample analysis[19,35]. However, systematic studies analyzing the percentage of cells with different identities infected by the virus and their susceptibility for SARS-CoV2 infection in human cortical organoid models at different stages *in vitro* are currently missing.

Here, we analyze neural cell infectivity of SARS-CoV2 in human cortical organoid models to understand the cellular tropism of the virus at different brain organoid maturation stages. We found that astrocytes, deep projection neurons, upper callosal neurons and inhibitory interneurons were infected by SARS-CoV2.

Astrocytes showed the highest rate of infected cells among the specific cell population in human cortical organoids at late stages *in vitro*. We detected low levels of *ACE2* expression but higher levels of some of its co-receptors, including *NRP1*, *CD147*, *GRP78*, *NRP2* and *AXL*, which may be involved in viral entry in the target cells. Mechanistically, we found that upon SARS-CoV2 infection, astrocytes undergo changes in morphology and upregulate SERPINA3, CD44 and S100A10 markers of astrogliosis, leading to broad adverse effects on cortical organoid cell populations by triggering an inflammatory response counteracted by upregulation of cell survival pathways.

MATERIALS AND METHODS

Human hCOs differentiation

Human cortical brain organoids (hCOs) were developed following a modified version of the Sasai lab protocol[37]. hESC-H9 cell line (WA09) (Metadata: Female, no disease associated) acquired from Wicell was used under the approval from the ethical committee from the University of Liège: Comité d'Ethique Hospitalo-Facultaire Universitaire de Liège (707) Reference: 2017-167. H9 cells were dissociated using Accutase (Stem Cell Technologies, 7922) and 9000 cells were seeded in 96-well U bottom plates (Nunclon sphere, 15396123) per well. Cells were cultured in DMEM-F12 with 20% KO serum (ThermoFisher), supplemented with NEAA, penicillin/streptavidin and 100µM β-mercaptoethanol (ThermoFisher) plus morphogens: 5µM SB (SB431542, Sigma, S4317) and 3µM IWR1 (Sigma, 681669) for 14 days. Rock inhibitor (Y-27632 2HC, Bio-Connect) was added until day 6 (20µM d0-d2, 10µM d2-d6). Organoids were cultured in DMEM-F12 medium supplemented with N2 (ThermoFisher, 17502048) and B27 (ThermoFisher, 11500446, 11530536) from day 14 and grown on orbital shakers (75 rpm) from day 21 and in bioreactor tubes (Bioké) from approximately day 46, speed 75 rpm. At day 70, 1% of matrigel (Corning, 11523550) was added to the culture. Medium was changed every 2 or 3 days.

SARS-CoV2 infection

All experiments have been conducted by the GIGA Viral platform (www.gigaviralvectors.uliege.be) in a Biosafety Level 3 lab under the environmental permit for GMO/pathogens related activities: EDII/1/1380C38/TL/pm. For the experiments we used the SARS-CoV2 strain (BetaCov/Belgium/GHB-03021/2020 (EPI ISL 407976|2020-02-03))[38] wild or recombinant SARS-CoV-2 strain harboring a mNeon-Green reporter[75]. VeroE6 cells were used to generate the SARS-CoV2 viral stock. Plaque assay method was used to determine the virus titer or plaque-forming unit (PFU)[32]. All SARS-CoV2 infections were performed for 3 hours followed by removal of the viral particles and a media change. Samples were analyzed following 24h, 72h or 2 weeks post-infection (long-stage post-infection).

RNA sequencing, data analysis and differential expression analysis

High quality RNA samples RIN values (8-10) were used for sequencing. Four samples of CTRL hCOs from 2 independent differentiations, and 4 samples from SARS-CoV2 72h post-infected hCOs from 2 different experiments were analyzed. The extracted RNA-seq libraries were generated by the GIGA Genomic platform (www.gigagenomics.uliege.be) using Illumina Stranded Total RNA Prep Ligation with Ribo-Zero Plus following the manufacturer protocol (Illumina ref: 20040529) and sequenced using the Illumina Novaseq 6000 sequencer, generating pair end 2x150bp reads. Downstream analysis was performed on R using DESeq2 method for normalization, clustering and differential expression analysis.

Statistical analysis

All statistical analysis were performed using GraphPad (Prism). All data were first tested for normality with a Shapiro-Wilcoxon test and based on the result of this test, the parametric or corresponding non-parametric version of the test was used. The test for multiple comparisons was chosen based on the recommendation from GraphPad Prism. All information concerning the test used and the multiple comparisons test applied are found in the legend of the corresponding figure.

RESULTS

SARS-CoV2 virus consistently infects human cortical organoids albeit at low levels

We aimed to test the infectivity and to identify the downstream effects of SARS-CoV2 viral infection in the human brain by means of an *in vitro* human cortical organoid model (hCO)[36,37]. For this purpose, hCOs[37] of 2, 3.5 and 5-6 months *in vitro* (2M, 3.5M, 5-6M) were incubated for 3h with SARS-CoV2 viruses[38] at a 0.5 multiplicity of infection (MOI) previously reported for assessing SARS-CoV2 infectivity of brain organoids[32], and analyzed 1 day (24h) or 3 days (72h) after infection (Fig. 1A). Immunolabelings of hCOs revealed the presence of SARS-CoV2 nucleocapside (NC) proteins in less than 0.1% of hCO cells (Fig. 1B-K and Movie S1). No difference was observed between the different hCO stages analyzed for the number of cells infected (NC+), nor between different times after infection (Fig. 1J). We reasoned that the exposition of hCOs to a higher viral load would result in increased cell infectivity. Our results showed that doubling the MOI of SARS-CoV2 exposure led to a higher level of infectivity of hCOs, suggesting that SARS-CoV2 infection follows a dose-dependent response (Fig. 1L-M). In contrast, and as expected, a similar approach using kidney Vero cells, a susceptible cell type for SARS-CoV2 infection[39], resulted in a higher level of infectivity at all SARS-CoV2 multiplicities of infection tested (Fig. S1). Next, we analyzed the level of expression of known SARS-CoV2 receptors and co-receptors in the hCOs. RNA sequencing of late stage

(6M) hCOs confirmed low expression of the major SARS-CoV2 receptor, *ACE2*[2,16,17], and higher expression of some of the SARS-CoV2 co-receptors such as *NRP1*, *CD147/BSG*; *GRP78/HSPA5*; *DPP4* and *AXL*[7,16,18–26] as well as some of the enzymes involved in the cleavage of the SARS-CoV2 virus spike protein to mediate viral entry to the cell, such as transmembrane serine protease 2 (*TMPRSS2*), cathepsin B (*CTSB*), cathepsin L (*CTSL*) and furin[14,23] (Fig. 1N). Immunolabelings confirmed the low/absence of expression of ACE2 in mouse cortex samples and in human brain organoids (Fig. S2A). In contrast, ACE2 expression was detectable in kidney Vero cells[39] (Fig. S2B). In agreement with our RNAseq data we could detect the expression of NRP1 in human brain organoids and in mouse cortex (Fig. S2C).

These results indicate that human cortical organoids are susceptible to infection by the SARS-CoV2 virus albeit at low levels, possibly due to the low levels of ACE2 present in the brain. Moreover, our results also suggest that some ACE2 co-receptors and proteases involved in entry of the SARS-CoV2 virus in the cells are expressed in human cortical organoids.

Deep layer projection neurons and astrocytes are the major cell types infected by SARS-CoV2 virus in hCOs at late stages *in vitro*

Next, we sought to analyze the cell identity of SARS-CoV2 infected cells in hCOs at different stages of maturation. First, we tested the infectivity of progenitors in hCOs from 2M up to 5-6M *in vitro*. Our experiments showed negligible numbers of either PAX6 or KI67 progenitor/proliferating cells infected by SARS-CoV2 in hCOs at any of the time points tested (Fig. S3A-D). Contrarily, we found that significant numbers of CTIP2+ deep layer projection neurons, and to a lesser extent CUX1+ upper layer callosal neurons were infected in hCOs at early (2M, 3.5M), and later (5-6M) time points (Fig. 2A-D). Strikingly, hCOs at later stages also showed a significant number of calbindin+ (CALB+) positive interneurons[40] and GFAP+ astrocytes infected (Fig. 2E-H). The overall analysis of the cell type identity among SARS-CoV2

infected cells in hCOs at 5-6M revealed that ~40% of the infected cells corresponded to GFAP+ and S100β+ astrocytes, followed by ~25% CTIP2+ cells, ~15% CALB+ cells and about ~3% CUX1+ cells (Fig. 2I and Fig. S3E). Further, we investigated which percentage of cells was infected among a specific cell type population in hCOs at 5-6 months. This analysis revealed that astrocytes were the cell type showing the highest percentage of cells infected among the total number of the specific cell population, when compared to excitatory and inhibitory neurons of the cortex (Fig. 2J and Fig. S3F).

These results suggest that SARS-CoV2 can infect astrocytes, deep projection neurons, upper callosal neurons and inhibitory neurons in the brain and identify astrocytes as the cell type with the highest susceptibility for infection in hCOs.

hCO cells infected with SARS-CoV2 do not undergo cell death

We asked whether SARS-CoV2 infectivity would lead to a higher rate of cell death in hCOs. To answer this question, we performed immunolabeling to detect activated cleaved-caspase 3 (CASP3) 24 hours or 72 hours post-exposure to SARS-CoV2, at different hCOs maturation stages in culture. Our analysis revealed no difference in the number of cleaved-CASP3 positive cells between infected and control hCOs (Fig. 3A-B, G-H). In agreement, higher MOI of SAR-CoV2 virus did not lead to a higher rate of apoptosis when compared to control hCOs (Fig. 3I). Moreover, almost no infected cells were found positive for cleaved-CASP3, further suggesting that the few apoptotic events detected were not SARS-CoV2-dependent (Fig. 3J). On the contrary, and as shown before, Vero cells showed high levels of cleaved-CASP3 following SARS-CoV2 exposure[41] (Fig. S4). Next, we sought to examine cell density as a global measurement of cell death in hCOs, as shown previously[42]. Our analysis showed no change in cell density following SARS-CoV2 infection neither when using higher SARS-CoV2 viral particle load (Fig. 3M-O). As we detected a preferential cell-type tropism for SARS-CoV2 virus combined with low levels of infectivity, we reasoned

that certain hCO cell populations could be more affected than others, and/or that effects on cell death could be present in a localized manner specifically around SARS-CoV2 infected areas in hCOs. However, we found no increased number of neurons CTIP2+ or astrocytes vimentin+ (VIM) co-labeled with CASP3 following SARS-CoV2 infection compared to control (Fig. 3C-F, K-L). In addition, we found no change in the percentage of proliferative progenitors (KI67+), deep and upper cortical layer neurons (CTIP2+, CUX1+) or interneurons (CALB+)[40] in SARS-CoV2 infected hCOs compared to control (Fig. S3G-J). Next, we measured cell density and nuclei area within SARS-CoV2 infected regions (NC+) to unravel localized cell death effects in hCOs. This analysis showed no difference in local cell death, neither following higher viral particle load (Fig. S5A-E), nor specifically on nuclei surrounding NC+ GFAP+ or NC+ S100β+ infected astrocytes (Fig. S5F-G), nor on GFAP+ or S100β+ nuclei surrounding NC+ cells (Fig. S5H-I).

These results overall suggest that infection by SARS-CoV2 does not trigger global, nor local, nor cell-type-dependent effects on cell death at the time points tested in hCOs.

SARS-CoV2 virus infects different brain regional identities *in vitro*

To test the tropism of SARS-CoV2 in the central nervous system, we infected human brain organoids with rostral and caudal regional identities. For this purpose, we generated brain organoids (BOs) with ventral telencephalic medial ganglionic eminences (MGE) identity, which are enriched in cortical interneurons and their progenitors[43–45]; BOs that model the thalamus (THL)[46]; and some that recapitulate features of the cerebellum (CRB)[47]. We exposed hCOs, MGE BOs, THL BOs and CRB BOs to SARS-CoV2 virus MOI 0.5 and measured its effects after 72h post-infection *in vitro*. Our analysis revealed that MGE BOs had the highest percentage of NC+ cells compared to hCOs, THL BOs or CRB BOs (Fig. 4A-G). Next, we measured the level of apoptosis-related events in those different brain regional identity BOs by measuring the percentage of cleaved-CASP3+ cells. This analysis revealed that SARS-CoV2 infected MGE BOs, THL BOs

and CRB BOs showed no difference in the percentage of cleaved-CASP3+ cells compared to controls, similarly to the previous data obtained with hCOs (Fig. 4H).

These results suggest that rostral forebrain telencephalic, diencephalic, and caudal hindbrain regions of the brain show susceptibility to SARS-CoV2 infection; with MGE identities showing the highest number of cells infected *in vitro*.

SARS-CoV2 infection in hCOs increases the expression of pro-inflammatory, pro-survival and astrogliosis-related genes

Next, we analyzed the overall impact of SARS-CoV2 infection on cell populations in hCOs. To address this, we analyzed 5-6M infected and control hCOs by bulk RNA sequencing to unravel genes and pathways affected following infection by SARS-CoV2. First, we validated the expression of SARS-CoV2 viral genes in infected hCOs (Fig. 5A). We did not detect statistical changes in the expression of SARS-CoV2 receptor and co-receptors following SARS-CoV2 infection of hCOs (Fig. S6A). Next, we analyzed genes differentially expressed between infected and control hCOs (p_{adj} <0.05). We found that several genes related to astrocyte-mediated inflammation and astrogliosis such as alpha-1 antichymotrypsin (*SERPINA3*)[50,51], S100 calcium binding protein A10 (*S100A10*)[52,53], homing cell adhesion molecule (*CD44*)[51,54–56], and the interleukin 13 receptor subunit alpha1 (*IL13RA1*), the immune system-related gene complement factor I (*CFI*), and the epidermal growth factor receptor (*EGFR*) were dysregulated following SARS-CoV2 infection in hCOs. In addition, the expression of lipid-metabolism related genes, which are associated to astrogliosis[48], such as phospholipase C-delta-3 (*PLCD3*) and phospholipase C-delta-1 (*PLCD1*) were also affected in infected hCOs. Interestingly, instead of effects promoting cell death pathways we detected an upregulation of the cell survival-related genes, such as superoxide dismutase 2 (*SOD2*)[57], brain and acute leukemia cytoplasmic protein (*BAALC*)[58-59], and the cytokine hepatocyte growth factor (*HGF*)[60] following

SARS-CoV2 infection (Fig. 5B-C and Table S1). Top candidate pathways (enrichR) and gene set enrichment analysis (GSEA) revealed the link of oxidative phosphorylation, glycolysis, TNFA signaling via NFKB, protein secretion, inflammatory responses, epithelial-mesenchymal transition, and lipid metabolism-related pathways (Fig. 5D-E, Fig. S6B and Tables S2 and S3). Interestingly, the expression of genes related to glycolysis and lipid metabolism, as well as the epithelial-mesenchymal transition pathway have been shown to be correlated with astrogliosis[48,49].

Next, we analyzed the impact of SARS-CoV2 infectivity on the astrocyte population since they are the most frequent cell type infected in hCOs. Our results showed that SARS-CoV2 infected hCOs had a lower GFAP+ organoid area coverage as compared to controls (Fig. 5F-I, L). While this phenotype did not result from the reduction in number of astrocytes in infected hCOs (Fig. 5M), our analysis revealed that SARS-CoV2 infected astrocytes had a reduced area as compared to control astrocytes (Fig. 5J-K, N).

Next, we further analyzed the expression of candidate pro-inflammatory *SERPINA3* and pro-survival *SOD2* genes in infected hCOs, as they could have important implications in the inflammatory cascades following SARS-CoV2 infection in hCOs. Our analysis revealed higher expression of the astrogliosis marker SERPINA3 and the pro-survival gene SOD2 in hCOs 72h post-infection compared to control (Fig. 6A-F, M). Moreover, we specifically found a higher percentage of astrocytes expressing SOD2 in hCOs 72h post-infection compared to control astrocytes, suggesting that astrocytes in infected hCOs switch on the expression of the *SOD2* gene as a mechanism against viral infection to promote anti-apoptotic pathways (Fig. 6G-I). In line with this observation, we found a lower percentage of cells labeled for gamma H2AX, a marker of DNA damage in the cell (Fig. 6J-L). Finally, we investigated the cellular effects triggered by SARS-CoV2 in hCOs 2 weeks long-stage (2W LS) post-infection (Fig. 7A). Two weeks LS hCOs had a trend for higher total number of NC+ cells (Fig. 7B-C, H) and increased number of GFAP+ NC+ and CTIP2+ NC+, however, no change in percentage of CTIP2+, nor GFAP+ infected cells among total NC+ cells was detected (Fig. 7B-C, I-J and Fig. S7A-B) when compared to 72h. These data suggest no change in cell type tropism but an overall

higher number of infected cells. No difference in cell death mechanisms such as CASP3+ cells for apoptosis (Fig. S7C-H, I-L), pMLKL+ cells for necroptosis[61] (Fig. S7M), nor difference in global or local cell density was detected in 2W LS hCOs compared to control or 72h (Fig. S7 N-P). In agreement with our previous results, we observed a reduction of GFAP+ hCO area in 2W LS (Fig. 7B-C, K). Remarkably, increased expression of CD44 and S100A10 was detected within the astrocyte population in 2W LS hCOs (Fig. 7D-G, L-N).

Overall, these results suggest that SARS-CoV2 infection triggers astrocyte morphological changes and increased expression of *SERPINA3*, *CD44* and *S100A10* astrogliosis-related genes. Moreover, SARS-CoV2 infection causes an overall increased expression of pro-inflammatory genes and upregulation of pro-survival pathways that may counteract cell death mechanisms thereby promoting resilience of dysregulated cells in hCOs.

DISCUSSION

The understanding of the ability of the SARS-CoV2 virus to infect the human brain has so far remained elusive due to the fact that only a few studies have reported the presence of viral RNA in CSF from COVID19 patients or detected the presence of the virus in postmortem brain samples[9,30,62-63]. However, neurological manifestations are present in about at least a third of COVID19 patients suggesting the possibility that pathological effects are triggered in the brain of patients[64]. Lack of SARS-CoV2 particle detection in the brain may result from the challenge to access CSF and/or brain tissue from COVID19 patients during critical phases of SARS-CoV2 infection, possibly combined with a low level of infectivity of SARS-CoV2 in the brain when compared to other tissues such as the respiratory system. In support of this hypothesis, a recent study based on 11 autopsies from COVID19 patients at different stages of the disease and using novel technologies for RNA detection (droplet digital PCR) succeeded in showing the presence of SARS-CoV2 RNA in 10 out of 11 of the brain samples analysed[10]. However, a limitation of this and similar

previous studies is that patient cohorts may have been more susceptible for SARS-CoV2 infectivity and its pathological downstream effects than control groups, due to preexistent unrelated medical conditions that finally led to their death from severe COVID-19. Moreover, previous concerns are the contamination of brain samples with blood cells or lung tissue during the autopsy procedure that could lead to false positive detection of SARS-CoV2. The aim of the current study is to analyze the ability of SARS-CoV2 to infect the brain, to distinguish its tropism towards different brain cell types, and to unravel major downstream effects of SARS-CoV2 infection in brain using a long-term human *in vitro* cortical organoid model.

The infectivity of SARS-CoV2 has been previously assessed in human telencephalic organoids derived from default differentiation paradigms and compared to that in choroid plexus organoids. This study found mostly infectivity of SARS-CoV2 restricted to choroid plexus cells with absence or minimum detection of virus RNA or protein in other brain organoid cell types[32]. Later reports using different brain organoid models reported however infectivity of the virus in brain cells besides choroid plexus cells[33,65–69]. Most of these studies reported a similar infectivity rate among cell types, including progenitors, neurons and glia cells, or on the contrary, higher infectivity in neurons[33,65–67,69-70]. Some recent studies have suggested a specific cellular tropism of SARS-CoV2 for astrocytes in the brain[19,35]. However, a systematic and quantitative analysis of brain cell types susceptible to SARS-CoV2 infection in brain organoids and the analysis of different brain organoid maturation stages *in vitro* including long-term cultures has not yet been performed. Here we present an exhaustive analysis of regionalized brain organoids at 3 different *in vitro* stages up to 6 months in culture exposed to SARS-CoV2 virus that reveals consistent infectivity of the virus at all stages albeit low levels (around 0.1%). This low percentage of infectivity in cortical organoids was consistent with the low level of detection of *ACE2* at the mRNA level. Nevertheless, we could detect higher expression of some of the ACE2 co-receptors such as NRP1 and DPP4 and some of the proteases involved in viral entry to the cell. In contrast with previous reports, we have not found infectivity of

progenitors or proliferative cells in hCOs at any of the maturation stages analyzed. Our analysis revealed a time-dependent pattern of tropism of the virus where at early stages deep projection neurons and upper callosal neurons were the most infected cell types whereas at late time points there was a switch towards astrocytes as the main target of the SARS-CoV2 virus. While the percentage of SARS-CoV2 infected cells represented around 0.1% of all hCO cells, SARS-CoV2 infected more than a 1% of the total astrocyte population at late stages *in vitro*, and this percentage was far higher than the one reported for any other infected cell type, suggesting a cell-type specific tropism of SARS-CoV2 for astrocytes.

In this study we have compared the efficiency of SARS-CoV2 to infect brain organoid models that mimic different regions of the forebrain and the developing cerebellum. Intriguingly, we found that ventral telencephalic organoids (MGE) were more susceptible to SARS-CoV2 infection as compared to other regionalized organoids. Other reports have previously interrogated the infectivity of SARS-CoV2 using multiple brain organoid regionalities *in vitro*, however, these studies did not reveal any difference in the percentage of infectivity between organoid models[33]. Our findings suggest that cortical interneurons and/or their progenitors could be important targets of SARS-CoV2 infection. Further work is needed to assess whether cortical interneurons that are traveling towards the cortex are also susceptible to SARS-CoV2 infection and whether this would affect their migration in forebrain assembloids[43–45].

The study of the downstream consequences of SARS-CoV2 infection in the brain has been the focus of several works for instance those reporting MRI scans-based brain abnormalities such as lesions in the white matter in COVID19 patients 6 months post-infection[27]. However, the extent of those brain anatomical alterations did not correlate with the neurological symptoms of the patients and there was an age mismatch between the control and infected group that could lead to the anatomical differences detected. Conversely, recent studies have found no major cytopathological effect outside the respiratory tract in postmortem patient samples[10]. Previous *in vitro* and *in vivo* studies have shown an increased cell death rate among SARS-CoV2 infected cells in the brain[9,19,35,71]. However, these results are in contrast with

other reports showing no major cell loss in different models[70,72]. We also aimed to clarify SARS-CoV2 downstream effects using cortical brain organoids at different stages *in vitro*. Our in-depth analysis showed no major effect on cell death, no change in apoptotic cell number, and no global, local or cell-type dependent change in cell density, or nuclei size in infected cortical organoids. Our RNAseq data from infected hCOs revealed overall increased expression of inflammatory and astrogliosis-related genes[51,54-56] such as *SERPINA3*, *CD44*, *S100A10*, increased oxidative phosphorylation, TNFA signaling, and metabolic changes, which suggests broad inflammatory-induced conditions in hCOs. Interestingly, we confirmed the upregulation of the astrogliosis markers SERPINA3, CD44 and S100A10 at the protein level in infected hCOs, suggesting that SARS-CoV2 infection may lead to astrogliosis in hCOs. Surprisingly, instead of cell death mechanism activation we detected upregulation of SOD2-related cell survival pathways, which suggest that compensatory pro-survival mechanisms are triggered in astrocytes and neuronal populations following SARS-CoV2 infection of hCOs. In agreement with this, we detected lower levels of DNA damage marked by H2AX gamma in hCOs infected by the virus, indicating possibly more efficient repair mechanisms for double strand DNA break. These results could imply the appearance of resilient dysregulated astrocytes and neurons within an inflammatory context following SARS-CoV2 infection.

Our current study comprises 2 short-term time points after SARS-CoV2 exposure of 1 and 3 days, and an additional long-stage (2 weeks) time post-infection to understand the immediate and late major cellular and transcriptomic changes occurring in brain cell types as a direct cause of the infection of the virus. Recent studies have attempted to decipher the pathological events in COVID19 patients suffering from SARS-CoV2-related symptoms beyond 3 months after exposure to the virus, which is known today as long-COVID[73]. It would be thus interesting in future studies to assess even longer-term effects in brain cell types following SARS-CoV2 infection in cortical organoid models.

Interestingly, some reports have hypothesized that SARS-CoV2-mediated effects in brain mimic the inflammatory conditions identified in the brains of patients suffering from neurodegenerative conditions[19,28,72]. Despite the limitation of our hCO model which lack major immune cell types, our results go in line with this hypothesis with pro-inflammatory changes triggered in our system only 1 to 3 days after infection of the virus combined with the activation of pro-survival pathways which could lead to survival of affected neurons and astrocytes. Strikingly, a known pro-inflammatory protein expressed in astrocytes, SERPINA3, which has been detected in plasma of middle-aged adults with high risk for dementia[74], was also upregulated in our infected cortical organoids. One could envision cortical brain organoids infected with SARS-CoV2 as an interesting model to study susceptibility to develop dementia-like features after long-term culture that could parallel the *in vivo* situation of neurodegenerative patients.

Lastly, we want to remark that we cannot exclude the occurrence of cell death events following longer SARS-CoV2 post-infection time points in hCOs. Besides, our model recapitulates the presence of human neurons and astrocytes but lacks the presence of microglia cells, which could have an important role in mediating cell death mechanisms following infection. Our current analysis used a restricted number of markers to identify specific cell populations, such as astrocytes, (GFAP+, S100β+ and VIM+), and few markers of astrogliosis to characterize the astrocyte response to the virus. Indeed, future studies using single cell technologies may unravel the full pattern of transcriptomic changes within astrocyte subpopulations following SARS-CoV2 infection.

In conclusion, we show here that hCOs at 3 different maturation stages *in vitro* up to 6 months present a reproducible level of low infectivity following SARS-CoV2 exposure. We demonstrate that astrocytes are the most representative cell type infected, and that this ultimately leads to increased astrogliosis-related

gene expression, pro-inflammatory and cell survival-related changes in the overall brain cell type populations in cortical organoids. These data unravel important pathways triggered in the brain following SARS-CoV2 infection that could be relevant for the design of future therapies aiming at protecting the brain from inflammatory dementia-like related pathological changes.

CONCLUSION

SARS-CoV2 infection leads to neurological symptoms in a subset of patients. Our study shows that SARS-CoV2 infects astrocytes, deep layer projection neurons, upper callosal neurons and interneurons of the cortex and trigger astrogliosis-related gene expression, overall inflammation and cell survival pathways.

These findings could imply the emergence of resilient dysregulated neurons and astrocytes in the context of an inflammatory environment. Our model could be instrumental for the design of future strategies aiming at lowering SARS-CoV2-related neurological effects.

ACKNOWLEDGEMENTS

This work was supported by the F.R.S.-FNRS #CUR 40002797 (to L. N. and I. E.-C.), and PER 40003579 (to L. N., I. E.-C., E. dV., J-C. T.). We thank the GIGA lentiviral Vectors, GIGA Imaging, and GIGA Genomics and Bioinformatics platforms for their contribution, help and support to this work.

DISCLOSURE OF POTENTIAL CONFLICTS OF INTERESTS

The authors declare no competing interests.

AUTHOR CONTRIBUTIONS

I.E-C designed the experimental plan. J-C.T and E.dV amplified the SARS-CoV2 virus and performed the SARS-CoV2 infections. M.C, I.E-C, I.C performed the experiments with the help of A.B, G.M and D.A. I.E-C, M.C, I.C analyzed all the results, I.E-C wrote the manuscript with the help of L.N, M.C, I.C and the rest of coauthors. I.E-C and L.N designed the initial study.

DATA AVAILABILITY STATEMENT

RNA sequencing data associated to this manuscript has been submitted to GEO with a submission ID: GSE250289

REFERENCES

1. Zhu, N., Zhang, D., Wang, W., Li, X., Yang, B., Song, J., Zhao, X., Huang, B., Shi, W., Lu, R., et al. (2020). A Novel Coronavirus from Patients with Pneumonia in China, 2019. N Engl J Med *382*, 727–733. 10.1056/NEJMoa2001017.
2. Kuba, K., Imai, Y., Rao, S., Gao, H., Guo, F., Guan, B., Huan, Y., Yang, P., Zhang, Y., Deng, W., et al. (2005). A crucial role of angiotensin converting enzyme 2 (ACE2) in SARS coronavirus-induced lung injury. Nat Med *11*, 875–879. 10.1038/nm1267.
3. Ding, Y., He, L., Zhang, Q., Huang, Z., Che, X., Hou, J., Wang, H., Shen, H., Qiu, L., Li, Z., et al. (2004). Organ distribution of severe acute respiratory syndrome (SARS) associated coronavirus (SARS-CoV) in SARS patients: implications for pathogenesis and virus transmission pathways. J Pathol *203*, 622–630. 10.1002/path.1560.
4. Puelles, V.G., Lütgehetmann, M., Lindenmeyer, M.T., Sperhake, J.P., Wong, M.N., Allweiss, L., Chilla, S., Heinemann, A., Wanner, N., Liu, S., et al. (2020). Multiorgan and Renal Tropism of SARS-CoV-2. N Engl J Med *383*, 590–592. 10.1056/NEJMc2011400.
5. Mao, L., Jin, H., Wang, M., Hu, Y., Chen, S., He, Q., Chang, J., Hong, C., Zhou, Y., Wang, D., et al. (2020). Neurologic Manifestations of Hospitalized Patients With Coronavirus Disease 2019 in Wuhan, China. JAMA Neurol *77*, 683. 10.1001/jamaneurol.2020.1127.
6. Helms, J., Kremer, S., Merdji, H., Clere-Jehl, R., Schenck, M., Kummerlen, C., Collange, O., Boulay, C., Fafi-Kremer, S., Ohana, M., et al. (2020). Neurologic Features in Severe SARS-CoV-2 Infection. N Engl J Med *382*, 2268–2270. 10.1056/NEJMc2008597.
7. Varatharaj, A., Thomas, N., Ellul, M.A., Davies, N.W.S., Pollak, T.A., Tenorio, E.L., Sultan, M., Easton, A., Breen, G., Zandi, M., et al. (2020). Neurological and neuropsychiatric complications of COVID-19 in 153 patients: a UK-wide surveillance study. Lancet Psychiatry *7*, 875–882. 10.1016/S2215-0366(20)30287-X.
8. Solomon, I.H., Normandin, E., Bhattacharyya, S., Mukerji, S.S., Keller, K., Ali, A.S., Adams, G., Hornick, J.L., Padera, R.F., and Sabeti, P. (2020). Neuropathological Features of Covid-19. N Engl J Med *383*, 989–992. 10.1056/NEJMc2019373.
9. Crunfli, F., Carregari, V.C., Veras, F.P., Silva, L.S., Nogueira, M.H., Antunes, A.S.L.M., Vendramini, P.H., Valença, A.G.F., Brandão-Teles, C., Zuccoli, G. da S., et al. (2022). Morphological, cellular, and molecular basis of brain infection in COVID-19 patients. Proc Natl Acad Sci U S A *119*, e2200960119. 10.1073/pnas.2200960119.
10. Stein, S.R., Ramelli, S.C., Grazioli, A., Chung, J.-Y., Singh, M., Yinda, C.K., Winkler, C.W., Sun, J., Dickey, J.M., Ylaya, K., et al. (2022). SARS-CoV-2 infection and persistence in the human body and brain at autopsy. Nature *612*, 758–763. 10.1038/s41586-022-05542-y.
11. Bartley, C.M., Johns, C., Ngo, T.T., Dandekar, R., Loudermilk, R.L., Alvarenga, B.D., Hawes, I.A., Zamecnik, C.R., Zorn, K.C., Alexander, J.R., et al. (2021). Anti-SARS-CoV-2 and Autoantibody Profiles in the Cerebrospinal Fluid of 3 Teenaged Patients With COVID-19 and Subacute Neuropsychiatric Symptoms. JAMA Neurol *78*, 1503–1509. 10.1001/jamaneurol.2021.3821.
12. Franke, C., Ferse, C., Kreye, J., Reincke, S.M., Sanchez-Sendin, E., Rocco, A., Steinbrenner, M., Angermair, S., Treskatsch, S., Zickler, D., et al. (2021). High frequency of cerebrospinal fluid autoantibodies in COVID-19 patients with neurological symptoms. Brain, Behavior, and Immunity *93*, 415–419. 10.1016/j.bbi.2020.12.022.

13. Placantonakis, D.G., Aguero-Rosenfeld, M., Flaifel, A., Colavito, J., Inglima, K., Zagzag, D., Snuderl, M., Louie, E., Frontera, J.A., and Lewis, A. (2020). SARS-CoV-2 Is Not Detected in the Cerebrospinal Fluid of Encephalopathic COVID-19 Patients. Front Neurol *11*, 587384. 10.3389/fneur.2020.587384.
14. Zhang, Y., Sun, S., Du, C., Hu, K., Zhang, C., Liu, M., Wu, Q., and Dong, N. (2022). Transmembrane serine protease TMPRSS2 implicated in SARS-CoV-2 infection is autoactivated intracellularly and requires N-glycosylation for regulation. J Biol Chem *298*, 102643. 10.1016/j.jbc.2022.102643.
15. Fuentes-Prior, P. (2021). Priming of SARS-CoV-2 S protein by several membrane-bound serine proteinases could explain enhanced viral infectivity and systemic COVID-19 infection. J Biol Chem *296*, 100135. 10.1074/jbc.REV120.015980.
16. Kyrou, I., Randeva, H.S., Spandidos, D.A., and Karteris, E. (2021). Not only ACE2-the quest for additional host cell mediators of SARS-CoV-2 infection: Neuropilin-1 (NRP1) as a novel SARS-CoV-2 host cell entry mediator implicated in COVID-19. Signal Transduct Target Ther *6*, 21. 10.1038/s41392-020-00460-9.
17. Xia, H., and Lazartigues, E. (2010). Angiotensin-converting enzyme 2: central regulator for cardiovascular function. Curr Hypertens Rep *12*, 170–175. 10.1007/s11906-010-0105-7.
18. Daly, J.L., Simonetti, B., Klein, K., Chen, K.-E., Williamson, M.K., Antón-Plágaro, C., Shoemark, D.K., Simón-Gracia, L., Bauer, M., Hollandi, R., et al. (2020). Neuropilin-1 is a host factor for SARS-CoV-2 infection. Science *370*, 861–865. 10.1126/science.abd3072.
19. Kong, W., Montano, M., Corley, M.J., Helmy, E., Kobayashi, H., Kinisu, M., Suryawanshi, R., Luo, X., Royer, L.A., Roan, N.R., et al. (2022). Neuropilin-1 Mediates SARS-CoV-2 Infection of Astrocytes in Brain Organoids, Inducing Inflammation Leading to Dysfunction and Death of Neurons. mBio *13*, e0230822. 10.1128/mbio.02308-22.
20. Gudowska-Sawczuk, M., and Mroczko, B. (2021). The Role of Neuropilin-1 (NRP-1) in SARS-CoV-2 Infection: Review. JCM *10*, 2772. 10.3390/jcm10132772.
21. Li, Y., Zhang, Z., Yang, L., Lian, X., Xie, Y., Li, S., Xin, S., Cao, P., and Lu, J. (2020). The MERS-CoV Receptor DPP4 as a Candidate Binding Target of the SARS-CoV-2 Spike. iScience *23*, 101160. 10.1016/j.isci.2020.101160.
22. Wang, S., Qiu, Z., Hou, Y., Deng, X., Xu, W., Zheng, T., Wu, P., Xie, S., Bian, W., Zhang, C., et al. (2021). AXL is a candidate receptor for SARS-CoV-2 that promotes infection of pulmonary and bronchial epithelial cells. Cell Res *31*, 126–140. 10.1038/s41422-020-00460-y.
23. Wang, K., Chen, W., Zhang, Z., Deng, Y., Lian, J.-Q., Du, P., Wei, D., Zhang, Y., Sun, X.-X., Gong, L., et al. (2020). CD147-spike protein is a novel route for SARS-CoV-2 infection to host cells. Sig Transduct Target Ther *5*, 283. 10.1038/s41392-020-00426-x.
24. Jackson, C.B., Farzan, M., Chen, B., and Choe, H. (2022). Mechanisms of SARS-CoV-2 entry into cells. Nat Rev Mol Cell Biol *23*, 3–20. 10.1038/s41580-021-00418-x.
25. Shin, W.-J., Ha, D.P., Machida, K., and Lee, A.S. (2022). The stress-inducible ER chaperone GRP78/BiP is upregulated during SARS-CoV-2 infection and acts as a pro-viral protein. Nat Commun *13*, 6551. 10.1038/s41467-022-34065-3.
26. Shin, J., Toyoda, S., Fukuhara, A., and Shimomura, I. (2022). GRP78, a Novel Host Factor for SARS-CoV-2: The Emerging Roles in COVID-19 Related to Metabolic Risk Factors. Biomedicines *10*, 1995. 10.3390/biomedicines10081995.

27. Offord, C. (2023). MRI study charts organ damage months after COVID-19. Science *381*, 1385. 10.1126/science.adl0645.
28. Yang, A.C., Kern, F., Losada, P.M., Agam, M.R., Maat, C.A., Schmartz, G.P., Fehlmann, T., Stein, J.A., Schaum, N., Lee, D.P., et al. (2021). Dysregulation of brain and choroid plexus cell types in severe COVID-19. Nature *595*, 565–571. 10.1038/s41586-021-03710-0.
29. Massimo, M., Barelli, C., Moreno, C., Collesi, C., Holloway, R.K., Crespo, B., Zentilin, L., Williams, A., Miron, V.E., Giacca, M., et al. (2023). Haemorrhage of human foetal cortex associated with SARS-CoV-2 infection. Brain *146*, 1175–1185. 10.1093/brain/awac372.
30. Lee, M.-H., Perl, D.P., Nair, G., Li, W., Maric, D., Murray, H., Dodd, S.J., Koretsky, A.P., Watts, J.A., Cheung, V., et al. (2021). Microvascular Injury in the Brains of Patients with Covid-19. N Engl J Med *384*, 481–483. 10.1056/NEJMc2033369.
31. Wenzel, J., Lampe, J., Müller-Fielitz, H., Schuster, R., Zille, M., Müller, K., Krohn, M., Körbelin, J., Zhang, L., Özorhan, Ü., et al. (2021). The SARS-CoV-2 main protease Mpro causes microvascular brain pathology by cleaving NEMO in brain endothelial cells. Nat Neurosci *24*, 1522–1533. 10.1038/s41593-021-00926-1.
32. Pellegrini, L., Albecka, A., Mallery, D.L., Kellner, M.J., Paul, D., Carter, A.P., James, L.C., and Lancaster, M.A. (2020). SARS-CoV-2 Infects the Brain Choroid Plexus and Disrupts the Blood-CSF Barrier in Human Brain Organoids. Cell Stem Cell *27*, 951-961.e5. 10.1016/j.stem.2020.10.001.
33. Jacob, F., Pather, S.R., Huang, W.-K., Zhang, F., Wong, S.Z.H., Zhou, H., Cubitt, B., Fan, W., Chen, C.Z., Xu, M., et al. (2020). Human Pluripotent Stem Cell-Derived Neural Cells and Brain Organoids Reveal SARS-CoV-2 Neurotropism Predominates in Choroid Plexus Epithelium. Cell Stem Cell *27*, 937-950.e9. 10.1016/j.stem.2020.09.016.
34. Wang, L., Sievert, D., Clark, A.E., Lee, S., Federman, H., Gastfriend, B.D., Shusta, E.V., Palecek, S.P., Carlin, A.F., and Gleeson, J.G. (2021). A human three-dimensional neural-perivascular "assembloid" promotes astrocytic development and enables modeling of SARS-CoV-2 neuropathology. Nat Med *27*, 1600–1606. 10.1038/s41591-021-01443-1.
35. Andrews, M.G., Mukhtar, T., Eze, U.C., Simoneau, C.R., Ross, J., Parikshak, N., Wang, S., Zhou, L., Koontz, M., Velmeshev, D., et al. (2022). Tropism of SARS-CoV-2 for human cortical astrocytes. Proc Natl Acad Sci U S A *119*, e2122236119. 10.1073/pnas.2122236119.
36. Magni, M., Bossi, B., Conforti, P., Galimberti, M., Dezi, F., Lischetti, T., He, X., Barker, R.A., Zuccato, C., Espuny-Camacho, I., et al. (2022). Brain Regional Identity and Cell Type Specificity Landscape of Human Cortical Organoid Models. Int J Mol Sci *23*, 13159. 10.3390/ijms232113159.
37. Kadoshima, T., Sakaguchi, H., Nakano, T., Soen, M., Ando, S., Eiraku, M., and Sasai, Y. (2013). Self-organization of axial polarity, inside-out layer pattern, and species-specific progenitor dynamics in human ES cell-derived neocortex. Proc Natl Acad Sci U S A *110*, 20284–20289. 10.1073/pnas.1315710110.
38. Spiteri, G., Fielding, J., Diercke, M., Campese, C., Enouf, V., Gaymard, A., Bella, A., Sognamiglio, P., Sierra Moros, M.J., Riutort, A.N., et al. (2020). First cases of coronavirus disease 2019 (COVID-19) in the WHO European Region, 24 January to 21 February 2020. Euro Surveill *25*, 2000178. 10.2807/1560-7917.ES.2020.25.9.2000178.
39. Zeng, C., Evans, J.P., King, T., Zheng, Y.-M., Oltz, E.M., Whelan, S.P.J., Saif, L.J., Peeples, M.E., and Liu, S.-L. (2022). SARS-CoV-2 spreads through cell-to-cell transmission. Proc Natl Acad Sci U S A *119*. 10.1073/pnas.2111400119.

40. Torres-Fernández, O., Yepes, G.E., Gómez, J.E., and Pimienta, H.J. (2005). Calbindin distribution in cortical and subcortical brain structures of normal and rabies-infected mice. Int J Neurosci *115*, 1375–1382. 10.1080/00207450590956396.
41. Ye, Z., Wong, C.K., Li, P., and Xie, Y. (2008). A SARS-CoV protein, ORF-6, induces caspase-3 mediated, ER stress and JNK-dependent apoptosis. Biochim Biophys Acta Gen Subj *1780*, 1383–1387. 10.1016/j.bbagen.2008.07.009.
42. Espuny-Camacho, I., Arranz, A.M., Fiers, M., Snellinx, A., Ando, K., Munck, S., Bonnefont, J., Lambot, L., Corthout, N., Omodho, L., et al. (2017). Hallmarks of Alzheimer's Disease in Stem-Cell-Derived Human Neurons Transplanted into Mouse Brain. Neuron *93*, 1066-1081.e8. 10.1016/j.neuron.2017.02.001.
43. Birey, F., Andersen, J., Makinson, C.D., Islam, S., Wei, W., Huber, N., Fan, H.C., Metzler, K.R.C., Panagiotakos, G., Thom, N., et al. (2017). Assembly of functionally integrated human forebrain spheroids. Nature *545*, 54–59. 10.1038/nature22330.
44. Bagley, J.A., Reumann, D., Bian, S., Lévi-Strauss, J., and Knoblich, J.A. (2017). Fused cerebral organoids model interactions between brain regions. Nat Methods *14*, 743–751. 10.1038/nmeth.4304.
45. Xiang, Y., Tanaka, Y., Patterson, B., Kang, Y.-J., Govindaiah, G., Roselaar, N., Cakir, B., Kim, K.-Y., Lombroso, A.P., Hwang, S.-M., et al. (2017). Fusion of Regionally Specified hPSC-Derived Organoids Models Human Brain Development and Interneuron Migration. Cell Stem Cell *21*, 383-398.e7. 10.1016/j.stem.2017.07.007.
46. Xiang, Y., Tanaka, Y., Cakir, B., Patterson, B., Kim, K.-Y., Sun, P., Kang, Y.-J., Zhong, M., Liu, X., Patra, P., et al. (2019). hESC-Derived Thalamic Organoids Form Reciprocal Projections When Fused with Cortical Organoids. Cell Stem Cell *24*, 487-497.e7. 10.1016/j.stem.2018.12.015.
47. Muguruma, K., Nishiyama, A., Kawakami, H., Hashimoto, K., and Sasai, Y. (2015). Self-organization of polarized cerebellar tissue in 3D culture of human pluripotent stem cells. Cell Reports *10*, 537–550. 10.1016/j.celrep.2014.12.051.
48. Xiong, X.-Y., Tang, Y., and Yang, Q.-W. (2022). Metabolic changes favor the activity and heterogeneity of reactive astrocytes. Trends Endocrinol Metab *33*, 390–400. 10.1016/j.tem.2022.03.001.
49. Vivinetto, A.L., Kim, I.-D., Goldberg, D.C., Fones, L., Brown, E., Tarabykin, V.S., Hill, C.E., Cho, S., and Cave, J.W. (2020). Zeb2 Is a Regulator of Astrogliosis and Functional Recovery after CNS Injury. Cell Rep *31*, 107834. 10.1016/j.celrep.2020.107834.
50. Zamanian, J.L., Xu, L., Foo, L.C., Nouri, N., Zhou, L., Giffard, R.G., and Barres, B.A. (2012). Genomic analysis of reactive astrogliosis. J Neurosci *32*, 6391–6410. 10.1523/JNEUROSCI.6221-11.2012.
51. Kim, H., Leng, K., Park, J., Sorets, A.G., Kim, S., Shostak, A., Embalabala, R.J., Mlouk, K., Katdare, K.A., Rose, I.V.L., et al. (2022). Reactive astrocytes transduce inflammation in a blood-brain barrier model through a TNF-STAT3 signaling axis and secretion of alpha 1-antichymotrypsin. Nat Commun *13*, 6581. 10.1038/s41467-022-34412-4.
52. King, A., Szekely, B., Calapkulu, E., Ali, H., Rios, F., Jones, S., and Troakes, C. (2020). The Increased Densities, But Different Distributions, of Both C3 and S100A10 Immunopositive Astrocyte-Like Cells in Alzheimer's Disease Brains Suggest Possible Roles for Both A1 and A2 Astrocytes in the Disease Pathogenesis. Brain Sci *10*, 503. 10.3390/brainsci10080503.

53. Fan, Y.-Y., and Huo, J. (2021). A1/A2 astrocytes in central nervous system injuries and diseases: Angels or devils? Neurochem Int *148*, 105080. 10.1016/j.neuint.2021.105080.
54. Taha, D.M., Clarke, B.E., Hall C.E., Tyzack G.E., Ziff, O.J., Greensmith, L., Kalmar B., Ahmed, M., Alarm A., Thelin, E.P., et al. (2022). Astrocytes display cell autonomous and diverse early reactive states in familial amyotrophic lateral sclerosis. Brain *145*, 481–489. 10.1093/brain/awab328.
55. Prakash, P., Erdjument-Bromge, H., O'Dea, M.R., Munson, C.N., Labib, D., Fossati, V., et al. (2024). Proteomic profiling of interferon-responsive reactive astrocytes in rodent and human. Glia *72*, 625–642. 10.1002/glia.24494.
56. Wu, P.-T., Su, W.-R., Li, C.-L., Hsieh, J.-L., Ma, C.-H., Wu, C.-L., Kuo, L.-C., Jou, I.-M., and Chen, S.-Y. (2019). Inhibition of CD44 induces apoptosis, inflammation, and matrix metalloproteinase expression in tendinopathy. J Biol Chem *294*, 20177–20184. 10.1074/jbc.RA119.009675.
57. Izuo, N., Nojiri, H., Uchiyama, S., Noda, Y., Kawakami, S., Kojima, S., Sasaki, T., Shirasawa, T., and Shimizu, T. (2015). Brain-Specific Superoxide Dismutase 2 Deficiency Causes Perinatal Death with Spongiform Encephalopathy in Mice. Oxid Med Cell Longev *2015*, 238914. 10.1155/2015/238914.
58. Weber, S., Alpermann, T., Dicker, F., Jeromin, S., Nadarajah, N., Eder, C., Fasan, A., Kohlmann, A., Meggendorfer, M., Haferlach, C., et al. (2014). BAALC expression: a suitable marker for prognostic risk stratification and detection of residual disease in cytogenetically normal acute myeloid leukemia. Blood Cancer J *4*, e173. 10.1038/bcj.2013.71.
59. Xu, B., Chen, G., Shi, P., Guo, X., Xiao, P., Wang, W., and Zhou, S. (2012). shRNA-Mediated BAALC knockdown affects proliferation and apoptosis in human acute myeloid leukemia cells. Hematology *17*, 35–40. 10.1179/102453312X13221316477499.
60. Xiao, G.H., Jeffers, M., Bellacosa, A., Mitsuuchi, Y., Vande Woude, G.F., and Testa, J.R. (2001). Anti-apoptotic signaling by hepatocyte growth factor/Met via the phosphatidylinositol 3-kinase/Akt and mitogen-activated protein kinase pathways. Proc Natl Acad Sci U S A *98*, 247–252. 10.1073/pnas.98.1.247.
61. Koper, M.J., Vasn Schoor, E., Ospitalieri, S., Vandenberghe, R., Vandenbulcke, M., Von Arnim, C.A.F., Tousseyn T., Balusu, S., et al. (2020). Necrosome complex detected in granulovacuolar degeneration is associated with neuronal loss in Alzheimer's disease. Acta Neuropathol. *139*, 463–484. 10.1007/s00401-019-02103-y.
62. Matschke, J., Lütgehetmann, M., Hagel, C., Sperhake, J.P., Schröder, A.S., Edler, C., Mushumba, H., Fitzek, A., Allweiss, L., Dandri, M., et al. (2020). Neuropathology of patients with COVID-19 in Germany: a post-mortem case series. Lancet Neurol *19*, 919–929. 10.1016/S1474-4422(20)30308-2.
63. Moriguchi, T., Harii, N., Goto, J., Harada, D., Sugawara, H., Takamino, J., Ueno, M., Sakata, H., Kondo, K., Myose, N., et al. (2020). A first case of meningitis/encephalitis associated with SARS-Coronavirus-2. Int J Infect Dis *94*, 55–58. 10.1016/j.ijid.2020.03.062.
64. Spudich, S., and Nath, A. (2022). Nervous system consequences of COVID-19. Science *375*, 267–269. 10.1126/science.abm2052.
65. Mesci, P., de Souza, J.S., Martin-Sancho, L., Macia, A., Saleh, A., Yin, X., Snethlage, C., Adams, J.W., Avansini, S.H., Herai, R.H., et al. (2022). SARS-CoV-2 infects human brain organoids causing cell death and loss of synapses that can be rescued by treatment with Sofosbuvir. PLoS Biol *20*, e3001845. 10.1371/journal.pbio.3001845.

66. Tiwari, S.K., Wang, S., Smith, D., Carlin, A.F., and Rana, T.M. (2021). Revealing Tissue-Specific SARS-CoV-2 Infection and Host Responses using Human Stem Cell-Derived Lung and Cerebral Organoids. Stem Cell Reports *16*, 437–445. 10.1016/j.stemcr.2021.02.005.
67. Song, E., Zhang, C., Israelow, B., Lu-Culligan, A., Prado, A.V., Skriabine, S., Lu, P., Weizman, O.-E., Liu, F., Dai, Y., et al. (2021). Neuroinvasion of SARS-CoV-2 in human and mouse brain. Journal of Experimental Medicine *218*, e20202135. 10.1084/jem.20202135.
68. Ramani, A., Pranty, A.-I., and Gopalakrishnan, J. (2021). Neurotropic Effects of SARS-CoV-2 Modeled by the Human Brain Organoids. Stem Cell Reports *16*, 373–384. 10.1016/j.stemcr.2021.02.007.
69. Zhang, B.-Z., Chu, H., Han, S., Shuai, H., Deng, J., Hu, Y., Gong, H., Lee, A.C.-Y., Zou, Z., Yau, T., et al. (2020). SARS-CoV-2 infects human neural progenitor cells and brain organoids. Cell Res *30*, 928–931. 10.1038/s41422-020-0390-x.
70. Wang, C., Zhang, M., Garcia, G., Tian, E., Cui, Q., Chen, X., Sun, G., Wang, J., Arumugaswami, V., and Shi, Y. (2021). ApoE-Isoform-Dependent SARS-CoV-2 Neurotropism and Cellular Response. Cell Stem Cell *28*, 331-342.e5. 10.1016/j.stem.2020.12.018.
71. Oh, J., Cho, W.-H., Barcelon, E., Kim, K.H., Hong, J., and Lee, S.J. (2022). SARS-CoV-2 spike protein induces cognitive deficit and anxiety-like behavior in mouse via non-cell autonomous hippocampal neuronal death. Sci Rep *12*, 5496. 10.1038/s41598-022-09410-7.
72. Beckman, D., Bonillas, A., Diniz, G.B., Ott, S., Roh, J.W., Elizaldi, S.R., Schmidt, B.A., Sammak, R.L., Van Rompay, K.K.A., Iyer, S.S., et al. (2022). SARS-CoV-2 infects neurons and induces neuroinflammation in a non-human primate model of COVID-19. Cell Reports *41*, 111573. 10.1016/j.celrep.2022.111573.
73. Davis, H.E., McCorkell, L., Vogel, J.M., and Topol, E.J. (2023). Long COVID: major findings, mechanisms and recommendations. Nat Rev Microbiol *21*, 133–146. 10.1038/s41579-022-00846-2.
74. Walker, K.A., Chen, J., Shi, L., Yang, Y., Fornage, M., Zhou, L., Schlosser, P., Surapaneni, A., Grams, M.E., Duggan, M.R., et al. (2023). Proteomics analysis of plasma from middle-aged adults identifies protein markers of dementia risk in later life. Sci Transl Med *15*, eadf5681. 10.1126/scitranslmed.adf5681.
75. Xie, X., Muruato, A., Lokugamage, K.G., Narayanan, K., Zhang, X., Zou, J., Liu, J., Schindewolf, C., Bopp, N.E., Aguilar, P.V., et al. (2020). An Infectious cDNA Clone of SARS-CoV-2. Cell Host Microbe *27*, 841-848.e3. 10.1016/j.chom.2020.04.004.

FIGURE LEGENDS

Figure 1: SARS-CoV2 infects human cortical organoids at different stages *in vitro*.

(A) Schematic illustration of the procedure followed for derivation of human cortical organoids of different stages *in vitro* (2M, 3.5M and 5-6M), hCO infection by SARS-CoV2 viral particles and subsequent analysis. Created with BioRender.com. (B-G) Tile-Scan (B,D,F) and single (C,E,G) confocal images of cryosections immunostained for the SARS-CoV2 antigen nucleocapside (NC, in red) in 72h SARS-CoV2 post-infection hCOs at all time points (2M, 3.5M, 5-6M). (H-I) Tile-Scan (H) and single (I) light-sheet microscope images of clarified (CUBIC) 72h SARS-CoV2 post-infected hCOs and immunostained for NC (in red) at 6M. Counterstaining was performed using DAPI. (J) Quantification of the percentage of NC+ cells among the total number of DAPI+ cells, in control (CTRL), 24h and 72h SARS-CoV2 post-infection hCOs at 2M, 3.5M and 5-6M *in vitro*. Data are represented as mean percentages ± SEM (3-4 differentiations: CTRL n=15-18; 24h n=6-12; 72h n=15-17). Two-way ANOVA with Tukey's multiple comparison test *p<0.05; **p<0.01; ****p<0.0001. (K) Quantification of the percentage of NC+ cells 72h post-infection in whole clarified (CUBIC) 72h SARS-CoV2 6M hCOs. Data are represented as mean percentages ± SEM (CTRL n=4; 72h n=5). Mann-Whitney test *p<0.05. (L) Tile-Scan and single immunofluorescence confocal images of the SARS-CoV2 antigen nucleocapside (NC, in red) in CTRL and following MOI 1 SARS-CoV2 infection in 3.5M hCOs. (M) Quantification of the percentage of NC+ cells in CTRL, MOI 0.5 and MOI 1 infected hCOs at 3.5M. Data are represented as mean percentages ± SEM (CTRL n=7; MOI 0.5 n=6; MOI 1 n=3). Kruskal-Wallis with Dunn's multiple comparison test *p<0.05; **p<0.01. (N) Expression levels (mean log) of SARS-CoV2 receptors and co-receptors (in green), and of SARS-CoV2 viral entry-related proteases (in orange) in 6M

hCOs (n=4) from bulk RNAseq. Data are represented as mean ± SEM. Scale bars: 100µm (B,D,F,L); 50µm (C,E,G); 300µm (H) and 40 µm (I).

Figure 2: SARS-CoV2 infects mostly astrocytes at late stages in hCOs.

(A,C,E,G) Tile-Scan (left panel) and single confocal images of cryosections immunostained for the SARS-CoV2 antigen nucleocapside (NC, in red) and the deep layer cortical neuronal marker CTIP2 (in green, A); the upper layer cortical neuronal marker CUX1 (in green, C); the interneuron marker calbindin (in green, E), or the astrocyte marker GFAP (in green, G) in 6M 72h post-infection hCOs, and high magnification insets. Counterstaining was performed using DAPI. (B,D,F,H) Quantification of the percentage of double positive CTIP2+ NC+ (B); CUX1+ NC+ (D); CALB+ NC+ (F); GFAP+ NC+ (H), among the total NC+ population in 2M, 3.5M and 5-6M 72h post-infected SARS-CoV2 hCOs compared to control (CTRL). Data are represented as mean percentages ± SEM (2-3 differentiations: CTRL n=8-20; 72h n=11-20). Two-way ANOVA with Tukey's multiple comparison test *p<0.05; **p<0.01; ****p<0.0001. (I) Percentage of specific cell types double positive for NC among the total NC+ population in 5-6M 72h post-infected SARS-CoV2 hCOs. Data are represented as mean percentages ± SEM (3-4 differentiations: 72h n=14-16). Two-way ANOVA with Tukey's multiple comparison test **p<0.01. (J) Percentage of NC+ infected cell type among the total number of the cell type-specific population in 5-6M 72h post-infected SARS-CoV2 hCOs. Data are represented as mean percentages ± SEM (3-4 differentiations: 72h n=15-20. Two-way ANOVA with Tukey's multiple comparison test *p<0.05; **p<0.01. Scale bars: 100µm (A,C,E,G). White arrows show cells double positive for NC and the specific cell-type marker tested (A,C,E,G).

Figure 3: SARS-CoV2 infectivity does not induce cell death in hCOs.

(A-F) Tile-Scan and single confocal images of cryosections immunostained for the apoptotic marker caspase 3 (CASP3)+ cells (in green) and either the SARS-CoV2 antigen NC (in red); the cortical layer V marker CTIP2; or the astrocyte marker VIM in 5-6M CTRL and 72h post-infected hCOs and high magnification pics (insets). Counterstaining was done with DAPI. (G-I) Quantification of the percentage of CASP3+ cells among the total number of cells DAPI+ in CTRL and 24h post-infected hCOs (G), in CTRL and 72h post-infected hCOs (H), or in CTRL, MOI 0.5 and MOI 1 (I) infected hCOs. Data are represented as mean percentages ± SEM (1-3 differentiations: 2M n= 12-18; 3.5M n=3-16; 5-6M n=6-15). Two-way ANOVA with Sidak's multiple comparison test (G-H) and one way ANOVA with Tukey's multiple comparison test (I). (J) Quantification of the percentage of double positive cells CASP3+ NC+ among the NC+ population. Data are represented as mean percentages ± SEM (3 differentiations: 2M n= 17-18; 3.5M n= 13-16; 5-6M n= 15). Two-way ANOVA with Tukey's multiple comparison test, ns: non-significant. (K-L) Quantification of the percentage of double positive cells CASP3+ CTIP2+ among CASP3 (K), and CASP3+ VIM+ among CASP3+ (L) at all stages. Data are represented as mean percentages ± SEM (1 differentiation: 2M n= 6; 3.5M n= 5; 5-6M n= 5). (G-K) Two-way ANOVA with Sidak's multiple comparison test, ns= non-significant. (M-O) Quantification of the cell density (number of DAPI cells per mm^2) in CTRL and 24h (M), CTRL and 72h (N), or in CTRL, MOI 0.5 and MOI 1 infected hCOs (O). (M-N) Data are represented as mean percentages ± SEM (3 differentiations: 2M n=12-17; 3.5M n=6-17; 5-6M n=12-17). Two-way ANOVA with Sidak's multiple comparison test. ns: non-significant. (O) Data are represented as mean percentages ± SEM (1 differentiation: CTRL n=7; MOI 0.5 n=6; MOI 1 n=3). One-way ANOVA test with Tukey's multiple comparison test ns: non-significant. Scale bars: 100µm (A-F).

Figure 4: **SARS-CoV2 virus infects different brain regional identity BOs *in vitro*.**

(A-F) Tile-Scan (A,C,E) and single (B,D,F) confocal images of cryosections immunostained for the SARS-CoV2 antigen nucleocapside (NC, in red) in 72h MGE BOs (A-B), THL BOs (C-D) and CRB BOs (E-F) at 2M. Counterstaining was performed using DAPI. (G) Quantification of the percentage of NC+ cells among the total number of cells DAPI+ in CTX hCOs, MGE BOs, CRB BOs and THL BOs. Data are represented as mean percentages ± SEM (CTX n=17; MGE n= 4; CRB n= 6; THL n=6). Kruskal-Wallis test with Dunn's multiple comparison test. *$p < 0.05$; **$p < 0.01$. (H) Quantification of the relative percentage of CASP3+ cells among the total number of cells DAPI+ in SARS-CoV2 infected CTX hCOs, MGE BOs, CRB BOs and THL BOs compared to CTRL CTX hCOs, MGE BOs, CRB BOs and THL BOs expressed as 1. Data are represented as normalized mean percentage ± SEM (CTX n=17; MGE n= 4; CRB n= 6; THL n=6). Kruskal-Wallis test with Dunn's multiple comparison test. Data were normalized by the mean value of control hCOs samples, ns: non-significant. Scale bars: 100µm (A-F).

Figure 5. SARS-CoV2 infection leads to astrocyte morphological changes and overall pro-inflammatory transcriptomic changes in hCOs.

(A) Heatmap representation of SARS-CoV2 normalized counts in CTRL or 72h SARS-CoV2 post-infected 5-6M hCOs. (B) Volcano plot representation of the changes in genes expression (DEG) in 5-6M 72h SARS-CoV2 post-infection hCOs compared to CTRL hCOs, representing the Log2foldChange (log_2FC) and the p_{adj} value ($-log_{10}FDR$). Genes with a p_{adj} value below 0.05 and with a negative Log2foldChange are represented in blue (downregulated genes), and genes with a p_{adj} value below 0.05 with a positive Log2foldChange are represented in red (upregulated). Genes that have a p_{adj} value above 0.05 are represented in grey (non-significantly changed). (C) Bar graph representation of the log fold change (lfc) of the differentially expressed genes in 72h post-infected hCOs compared to CTRL hCOs. In red: Astrocyte-mediated inflammatory genes; in green: lipid metabolism-related genes; in blue: cell survival-related genes. (D)

Representation of the top pathways from MSigDB Hallmark pathways database based on the significance of enrichment of upregulated and downregulated DEGs. (E) Bubble plot of the Gene Set Enrichment Analysis (GSEA) representing the enriched pathways with a p_{adj} value < 0.0001. Pathways that have a normalized enrichment score (NES) positive >0 are upregulated whereas pathways with a NES negative <0 are downregulated. Pathways were ordered by the NES score in a decreasing manner. Size represented the number of genes from the RNAseq presented in the pathway. All data were generated from bulk RNAseq analysis of 2 independent differentiations (CTRL n=4; 72h n=4). *p < 0.05; **p < 0.01; ***p < 0.001; ****p < 0.0001. (F-K) Tile-Scan (F-I) and single (J-K) confocal images of cryosections immunostained for the astrocyte marker GFAP (in green: F-I; black and white mask: J-K) in 5-6M CTRL and 72h post-infected hCOs. Counterstaining was performed using DAPI. (L) Percentage of organoid area covered by GFAP+ cells in CTRL and 72h hCOs of 2M, 3.5M and 5-6M. Data are represented as mean percentages ± SEM (2-4 differentiations: 2M n= 6-12; 3.5M n= 6-11; 5-6M n= 12-22). Two-Way ANOVA with Sidak's multiple comparison test **p<0.01. (M) Quantification of the percentage of GFAP+ cells among the total number of cells DAPI+ in CTRL and 72h post-infected 5-6M hCOs. Data are represented as mean percentages ± SEM (4 differentiations: CTRL n= 23; 72h n=20). Mann-Whitney two-tailed test * p<0.05. (N) Quantification of astrocyte area in CTRL and 72h post-infected 5-6M hCOs. Data are represented as mean percentages ± SEM, (4 differentiations: CTRL n= 22 organoids; 72h n=22 organoids). Mann-Whitney two-tailed test * p<0.05. Scale bars 500µm (F-G); 100 µm (H-I); 25µm (J-K). Red arrows show examples of representative astrocytes (E,F).

Figure 6. Increased expression of astrogliosis-related markers and pro-survival genes in infected hCOs.

(A-B,D-E,G-H,J-K) Tile-Scan and single confocal images of cryosections immunostained for the astrogliosis marker SERPINA3 (in green; A-B), the pro-survival gene SOD2 (in green; D-E, G-H), the astrocyte marker

GFAP (in red; G-H), and the DNA double strand break marker gamma H2AX (in green; J-K) in 5-6M CTRL and 72h post-infected hCOs. Counterstaining was performed using DAPI. White arrows show cells double positive for SOD2 and GFAP (H). (C,F,I,L) Quantifications of the percentage of SERPINA3+ (C), SOD2+ (F), SOD2+ GFAP+ (I) and gamma H2AX+ (L) cells over the total number of DAPI+ in control and 72h post-infected 5-6M hCOs. Data are represented as mean percentages ± SEM (4 differentiations: CTRL n= 20; 72h n=20). (C,F) Mann-Whitney test **p<0.01; ***p<0.001 (I) Mann-Whitney test **p<0.01. (L) Two-tailed t-test *p<0.05. (M) Western blot detection of SERPINA3 and β-actin levels from protein extracts of CTRL and 72h infected hCOs. MW for SERPINA3 is aprox. 52 and 60 kDa. Quantification of the levels of SERPINA3 in CTRL and 72h post-infected hCOs normalized with β-actin levels. Data are represented as mean value ± SEM (2 differentiations, 3 replicates (n=8 organoids/sample). T-test *p < 0.05. Data were normalized by the mean value of control hCOs samples. Scale bars: 500µm (A-K) and 50 µm (higher magnification views on the right).

Figure 7. Long-stage post-infected hCOs show changes in GFAP hCO coverage and upregulation of CD44 and S100A10 astrogliosis markers.

(A) Schematic illustration of the procedure followed for hCO infection by SARS-CoV2 and analysis after long-stage post-infection (2 weeks). Created with BioRender.com. (B-G) Tile-Scan (B-C) and single (D-G) confocal images of cryosections immunostained for the SARS-CoV2 antigen nucleocapside (NC, in red; B-C) and GFAP (in green; B-E), CD44 (in red; D-E), VIM (in red; F-G) and S100A10 (in green; F-G) in LS SARS-CoV2 post-infected hCOs of 6M. Counterstaining was performed using DAPI. (H-J) Quantification of the percentage of NC+ cells (H), the percentage of NC+ CTIP2+ (I) or NC+ GFAP+ (J), among the total number of DAPI+ in control 72h (CTRL 72h), control LS (CTRL LS), 72h SARS-CoV2 post-infected (72h) and LS 2weeks post-infected (2W LS) hCOs at 6M *in vitro*. Data are represented as mean percentages ± SEM (2-4

differentiations: CTRL 72h n= 15; CTRL LS n=11; 72h n=15; 2W LS n=9). Kruskal-Wallis with Dunn's multiple comparison test *p<0.05; **p<0.01; ****p<0.0001. (K-L, N) Quantification of GFAP+ area (K), the CD44+ area (L), and the S100A10+ area (N) in CTRL LS and 2W LS 6M hCOs. Data are represented as mean percentages ± SEM. (2 differentiations: CTRL LS n= 11; 2W LS n=9). T-test (K-L), Mann-Whitney two-tailed test (N) *p<0.05; **p<0.01. (M) Quantification of CD44+ GFAP+ cells in CTRL LS and 2W LS 6M hCOs. Data are represented as mean percentages ± SEM. (2 differentiations: CTRL LS n= 11; 2W LS n=9). Mann-Whitney two-tailed test ***p<0.001. Data were normalized by the mean value of control hCOs samples. Scale bars: 100µm.

Figure 1

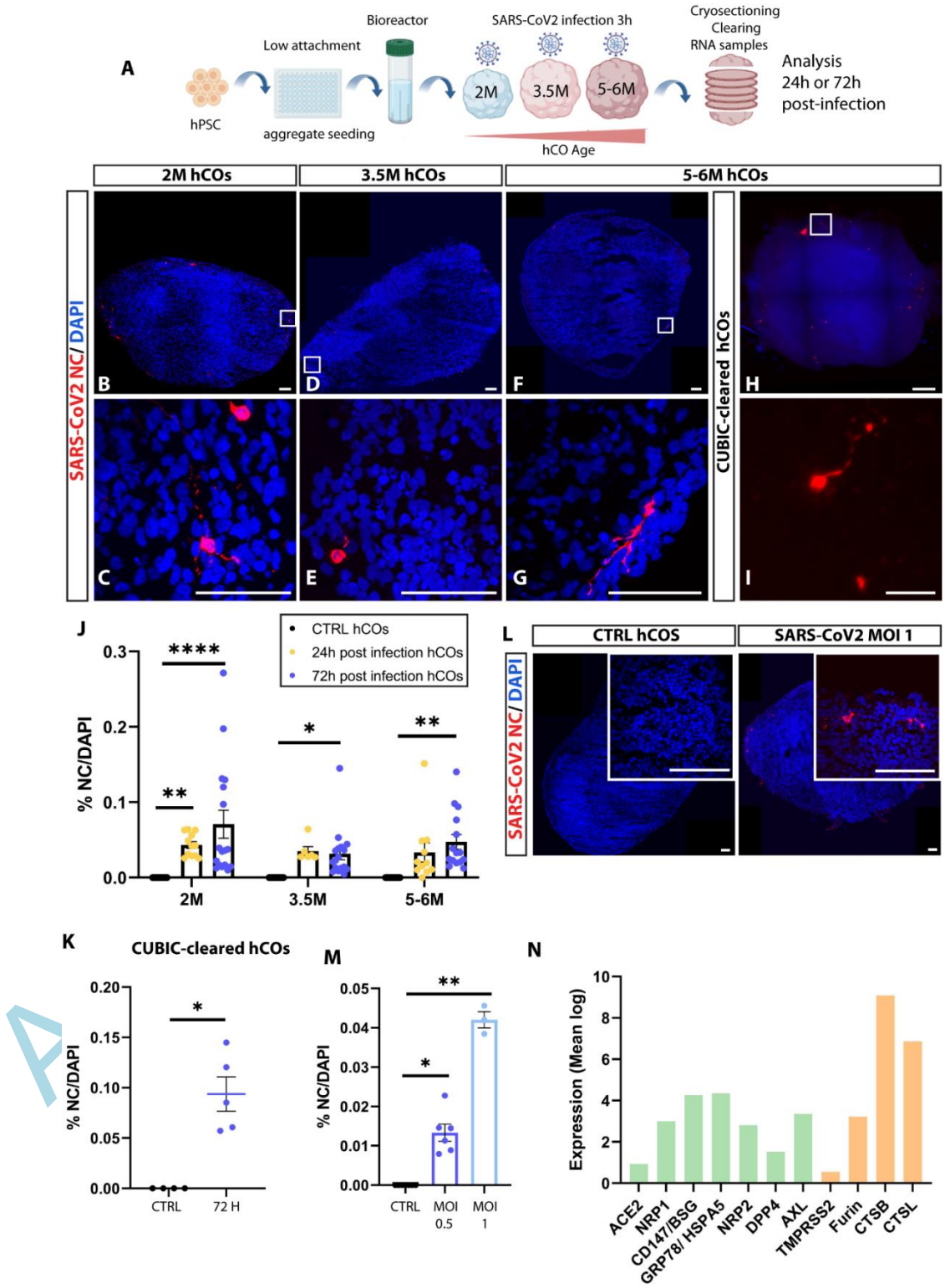

Figure 2

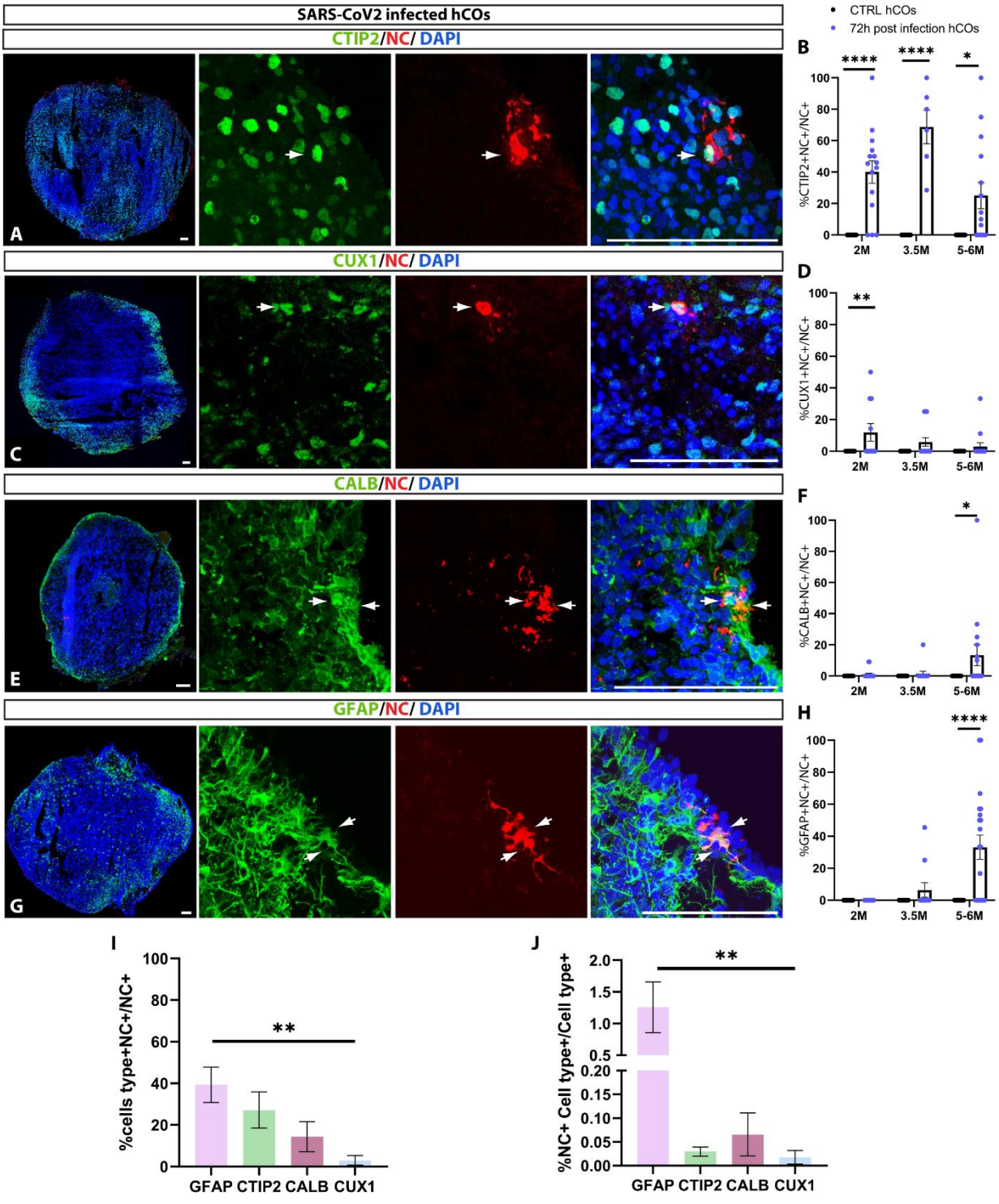

Figure 3

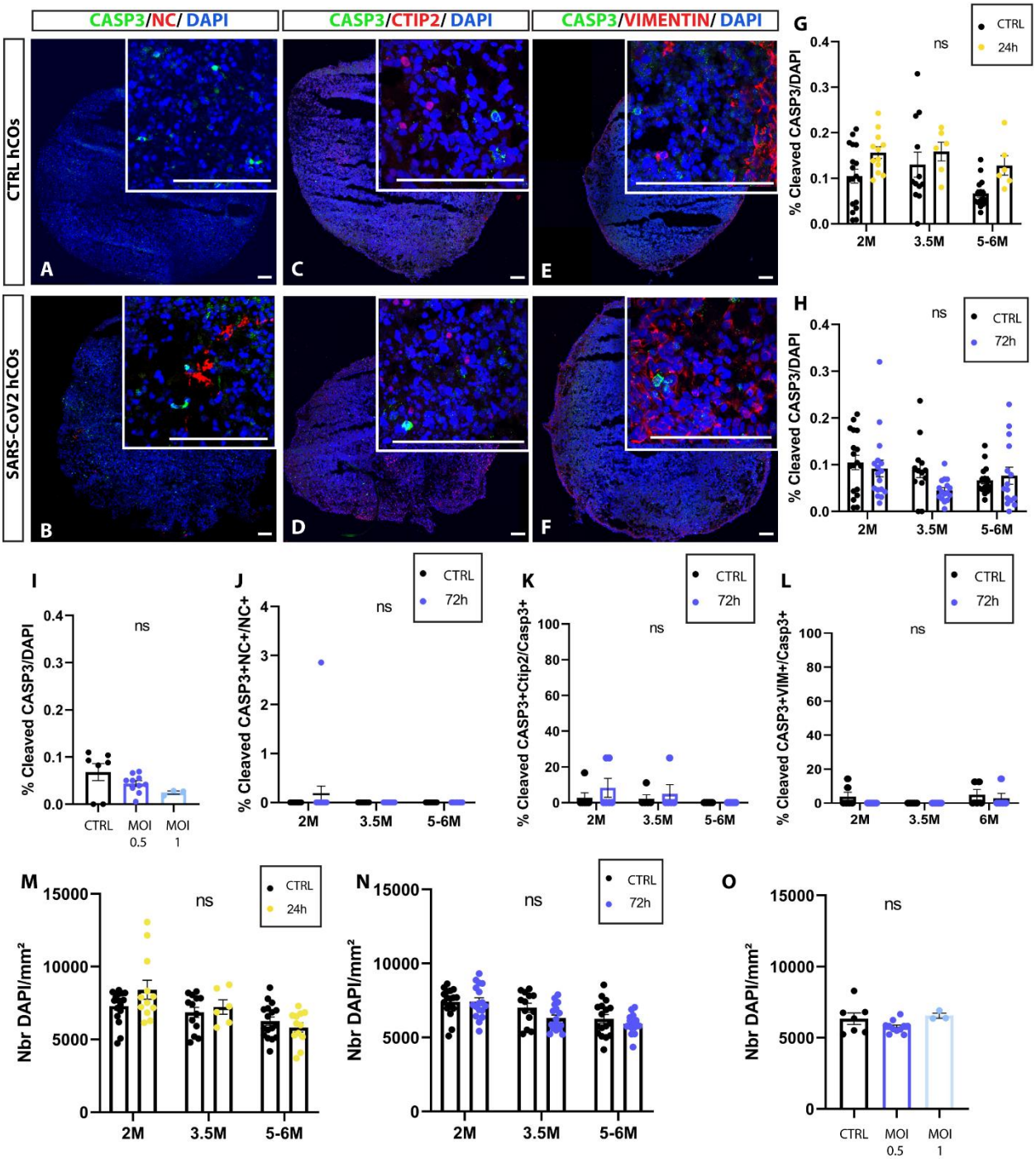

Figure 4

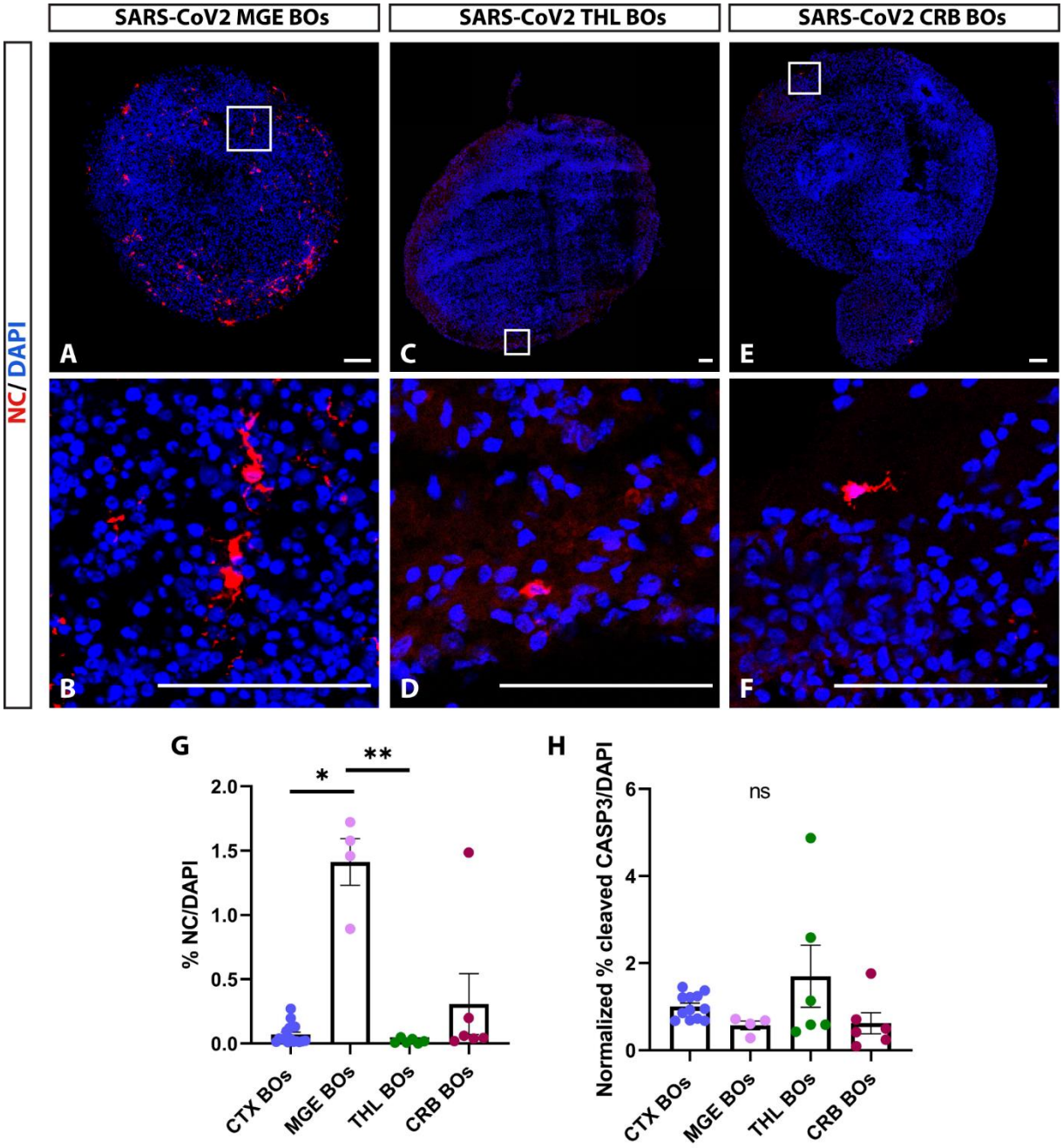

Figure 5

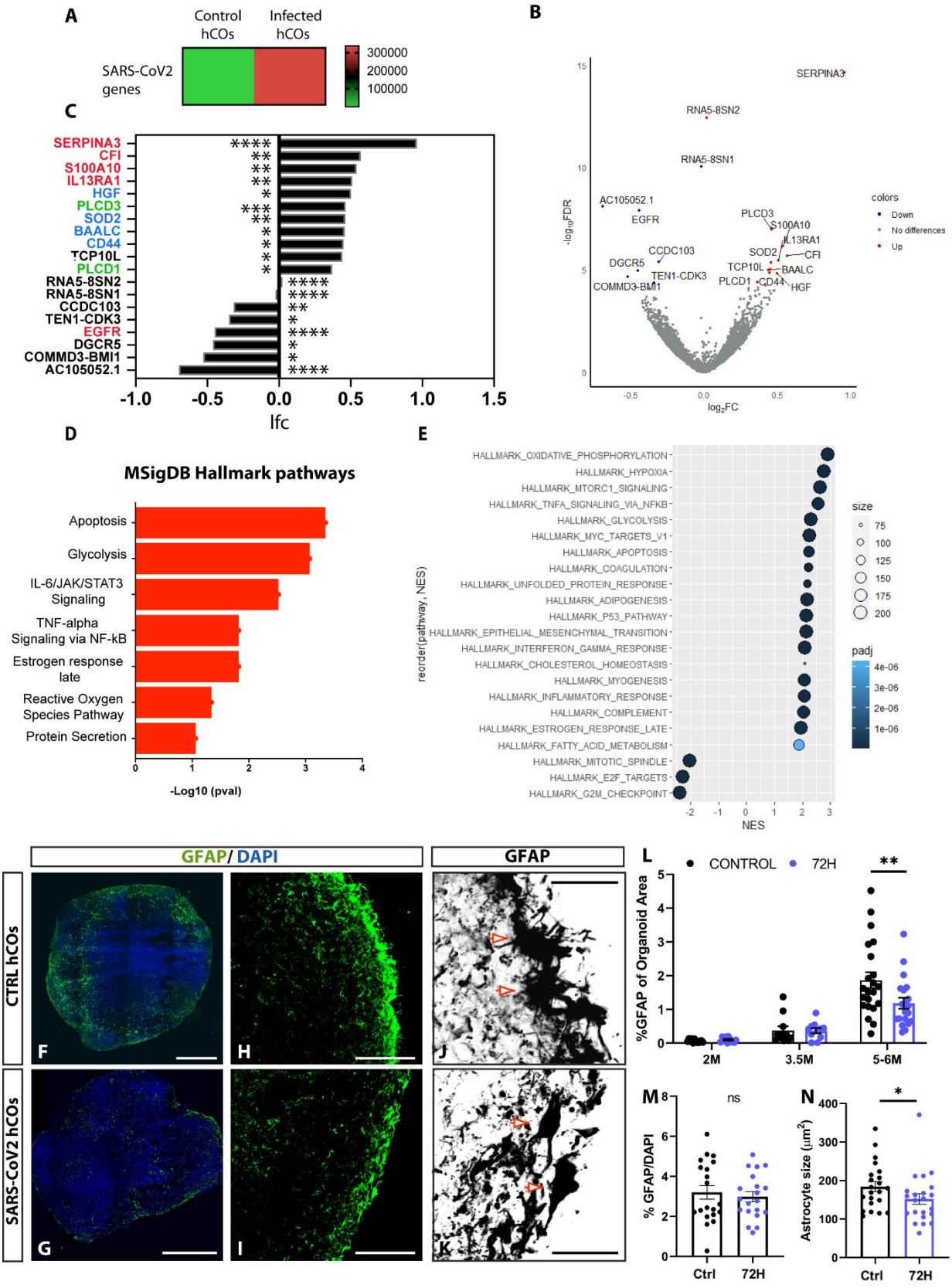

Figure 6

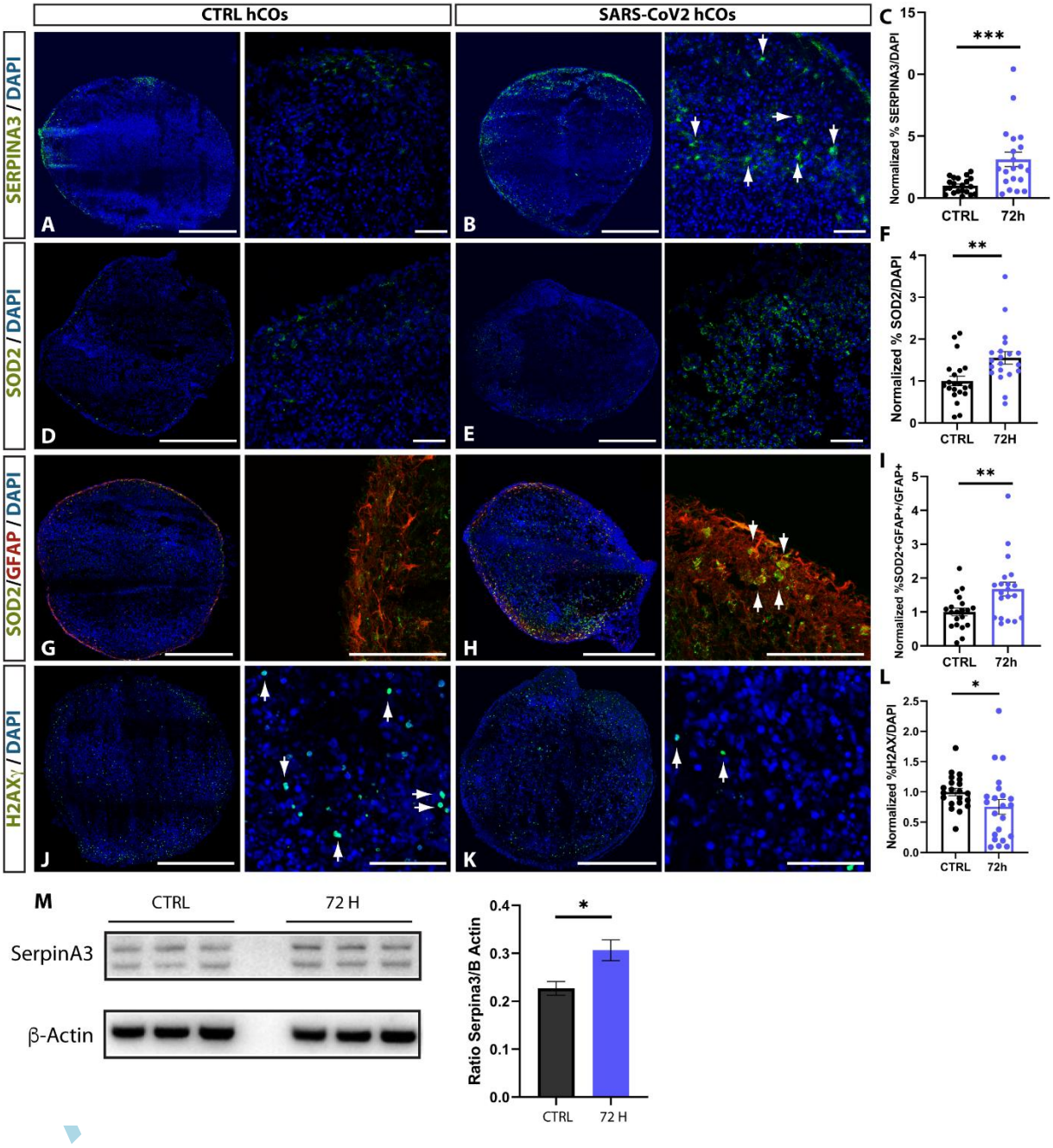

Figure 7